Extreme small-scale clustering of droplets in turbulence driven by hydrodynamic interactions

Extreme Small-Scale Clustering of Droplets in Turbulence Driven by Hydrodynamic Interactions

M. A. Yavuz, R. P. J. Kunnen,* G. J. F. van Heijst, and H. J. H. Clercx
Fluid Dynamics Laboratory, Department of Applied Physics and J. M. Burgers Center for Fluid Dynamics, Eindhoven University of Technology, P.O. Box 513, 5600 MB Eindhoven, The Netherlands
(Dated: May 24, 2018)

We perform three-dimensional particle tracking measurements on droplets in a turbulent airflow. The droplets display the well-known preferential concentration of inertial particles, with an additional extreme clustering at the smallest scales. We explain this additional clustering phenomenon theoretically based on a Stokes-flow description of two spheres including their mutual hydrodynamic interaction and a perturbative small-inertia expansion.

Small, heavy particles in a turbulent flow display clustering [1–9]. This process, known as preferential concentration, enhances collision probability and can, thereby, for example, accelerate coalescent growth of raindrops [10–12]. Here we show with experiments that droplets in a turbulent airflow display an additional and quantitatively highly significant clustering effect at length scales even smaller than the smallest flow length-scale (the Kolmogorov length) due to hydrodynamic interaction, thus further enhancing the collision probability. We rationalize this observation with an analytical study employing the Stokes-flow description of two interacting tracer particles [13, 14] with a perturbative expansion of inertial effects [5], revealing that the observed small-scale clustering is indeed a result of hydrodynamic interaction. Inertial particles in turbulence are typically modelled disregarding hydrodynamic interactions entirely, or at best by parametrizing the well-known Stokes solution for viscous flow past a sphere to emulate the resulting disturbance flow on a test particle [15–17]. However, the latter approach disregards the proper boundary condition on the particles and so does not realistically represent the near-field flow at all. Current models for precipitation formation underpredict the speed of raindrop growth [10–12]. The extra clustering described here significantly enhances the collision probability; adoption of this effect in the models will result in more accurate predictions.

Droplet clustering can be quantified with the radial distribution function (RDF) $g(r)$ [18], a measure of the probability of finding a particle at a separation r from a test particle in comparison to that probability in a uniform distribution, for which $g = 1$. Higher values $g(r) > 1$ indicate clustering. The RDF for weakly inertial non-interacting particles in turbulence is a power-law, $g \propto r^{-\alpha}$ with exponent α a function of the turbulent flow and particle properties [5]. This power-law behaviour is confirmed in direct numerical simulations [19] (DNS) and experiments [6, 8]. However, our current experiment using three-dimensional (3D) droplet tracking allows us to determine the RDF to considerably smaller separations r than before, leading to the observation of an additional clustering mechanism which is not modelled in the DNS and not resolved in earlier experiments.

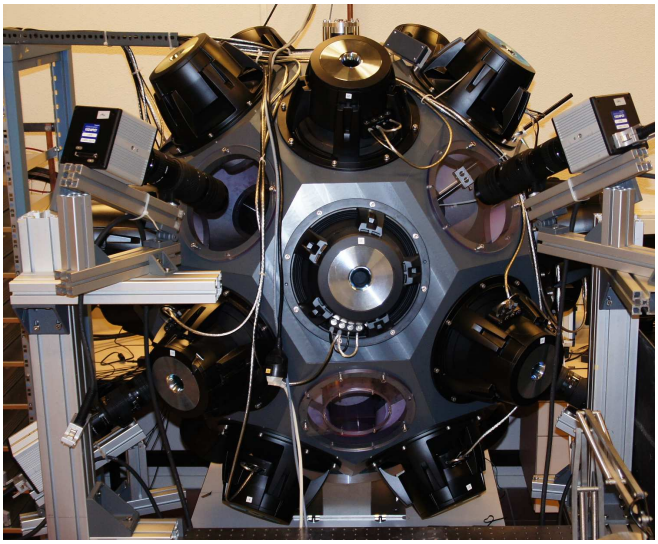

FIG. 1. Turbulence chamber with 20 loudspeakers to drive the turbulent airflow. Four cameras (top left, bottom left, top right and bottom right (behind the bar)) are mounted in front of windows to track the droplet motion; laser illumination is provided through the lower central window.

In the experiments turbulence is generated in a soccer-ball-shaped chamber, inspired by [20–22], with a mean diameter of 1 m (Fig. 1). Twenty loudspeakers are mounted in the hexagonal plates of the truncated icosahedron; the twelve pentagons are used for optical access and mounting. The loudspeakers drive synthetic jets which create tunable turbulence with good homogeneity and isotropy in the center; speaker pairs move in anti-phase to prevent pressurizing. The turbulence is characterized with particle image velocimetry and dedicated post-processing [23] is used to obtain the dissipation rate ϵ, the Taylor-scale Reynolds number Re_λ, and the Kolmogorov length (η) and time (τ_η) scales. Three flow settings are used here, detailed in Table I.

Water droplets are added with a spinning-disk aerosol generator [22, 24, 25]. This device produces many

TABLE I. Turbulence and droplet characteristics. Included are: the Taylor-scale Reynolds number Re_λ, dissipation rate ϵ, Kolmogorov length η, Kolmogorov time τ_η, and the Stokes numbers St for the three different droplet sizes. Error intervals denote one standard deviation.

Re_λ	ϵ	η	τ_η	droplet radius a (μm)		
	($\mathrm{m}^2/\mathrm{s}^3$)	(mm)	(ms)	7.1 ± 0.3	10.0 ± 0.6	20.7 ± 0.7
				corresponding St		
155	0.30	0.33	7.1	0.09 ± 0.01	0.19 ± 0.02	0.84 ± 0.04
229	2.1	0.20	2.7	0.22 ± 0.01	0.46 ± 0.04	2.02 ± 0.10
314	9.7	0.14	1.2	0.49 ± 0.03	0.99 ± 0.08	4.38 ± 0.21

droplets with a narrow size distribution, measured using interferometric particle imaging [26]. Three different droplet radii a are applied here: $a = 7$, 10, and 21 μm. Table I lists the widths of the distributions of a and the corresponding Stokes numbers $\mathrm{St} = \tau_p/\tau_\eta$; the relaxation time $\tau_p = \frac{2}{9}\rho_p a^2/\mu$ with ρ_p the density of the droplets (water) and μ the dynamic viscosity of air. The Stokes number quantifies the importance of inertial forces on the droplet motion; ideal flow tracers have $\mathrm{St} = 0$. It is customary to use the settling factor $\mathrm{Sv} = \tau_p a_g/u_\eta$, with a_g the gravitational acceleration and $u_\eta = \eta/\tau_\eta$ the Kolmogorov velocity, to quantify the relative importance of gravity [27, 28]. In our current experiments we obtain values $0.05 < \mathrm{Sv} < 1.3$, implying that the role of gravity is small compared to that of turbulence [27–29]. In particular, $\mathrm{Sv}_{\mathrm{rms}} = \tau_p a_g/u' \ll 1$, where u' is the root-mean-square (rms) flow velocity. The volume fraction of droplets is at most $\phi_v \approx 3 \times 10^{-5}$ for some experiments with the largest droplets and smaller otherwise, meaning that the experimental conditions are dilute: the so-called one-way coupling regime [9, 30] where dynamics of particles can be globally described disregarding particle–particle interactions and particles do not significantly affect the turbulence.

We apply particle tracking velocimetry (PTV) to the droplets in a central volume of approximate dimensions $25 \times 25 \times 25$ mm^3. This volume is illuminated with a pulsed Nd:YLF laser (Spectra-Physics Empower 45, frequency 1 kHz) with an expanded beam guided through the measurement volume three times using mirrors. Four cameras (Photron FastcamX-1024PCI, resolution 1 Mpixel, frequency 1 kHz) record the motion of the droplets in the measurement volume. The PTV algorithm developed at ETH Zürich (Switzerland) [31–33] is applied to recover 3D droplet trajectories. Subsequent cubic polynomial smoothing [33] reduces measurement noise considerably. The median position displacement due to filtering is considerably less than 1 pixel size.

3D droplet position snapshots are reproduced from the trajectories, restricting the interrogation volume V to a central sphere of radius 10 mm. These snapshots are used to calculate the RDF (by binning of droplet pairs according to their separation distance) as [6]

$$g(r_i) = \frac{N_i/\Delta V_i}{N/V}\,, \tag{1}$$

where N_i is the number of pairs found with separation $r_i \pm \Delta r_i/2$, ΔV_i the intersection volume of the spherical shell (with mean radius r_i around the reference droplet and exponentially increasing thickness Δr_i) and V, N the total number of pairs within V, and i the bin index. The total number of detected particle pairs in a given experiment varies between 8×10^3 for $a = 21$ μm and $\mathrm{Re}_\lambda = 314$ and 5×10^6 for $a = 10$ μm and $\mathrm{Re}_\lambda = 155$. The number of bins (and hence the bin width) per experiment is chosen based on the number of detected pairs; when less droplet pairs are detected it is required to apply wider bins to attain converged RDFs. Measurements last between 150 and 700 integral timescales $T = \frac{3}{2}(u')^2/\epsilon$; details on duration, statistical convergence and computation of the RDF error bars are given in the Supplemental Material [34].

The measured RDFs are plotted in Fig. 2. Note that the horizontal axis is normalized with droplet radius a rather than the Kolmogorov length η as is customary; this choice supports the analysis of the hydrodynamic interaction terms which are series expansions in terms of a/r. Each RDF curve displays a drop-off at the largest separations r, resembling the results of Ref. [8], where this effect is attributed to imperfect large-scale mixing of droplets. At intermediate r we recover the well-known power-law scaling. At small r, however, all RDFs reach values which are up to two orders of magnitude higher than expected from the pure power law. The main reason that we are the first to report this effect and raise the awareness of the role of hydrodynamic interaction is that the current measurement technique gives access to resolved statistics at smaller separations r than in earlier experiments [6, 8] given the long averaging times [34]. In the current experiment we can confidently resolve droplet separations down to at least $r/\eta = 0.2$ in all cases except for at $\mathrm{Re}_\lambda = 314$ and $\mathrm{St} = 0.49$ ($r/\eta \geq 1$) or 4.38 ($r/\eta \geq 0.6$), where the smaller number of detected pairs significantly reduces statistical convergence at the smallest r. Previous works [6, 8] could only report converged data down to $r/\eta \approx 1$. In fact, in hindsight there is preliminary evidence of a steeper scaling at small r than at larger separations in the earlier holographic 3D measurement [6]. Previous studies considered clustering of electrically charged particles [35, 36]; however, this effect cannot explain the currently observed trends in clustering [37]. We shall instead argue that the strong enhancement of the RDF is the effect of hydrodynamic interaction (HI) based on a theoretical description detailed in the Supplemental Material [34], summarized in what follows.

Consider two small spherical particles with radius $a \ll \eta$ in a turbulent flow. Their relaxation time τ_p is as-

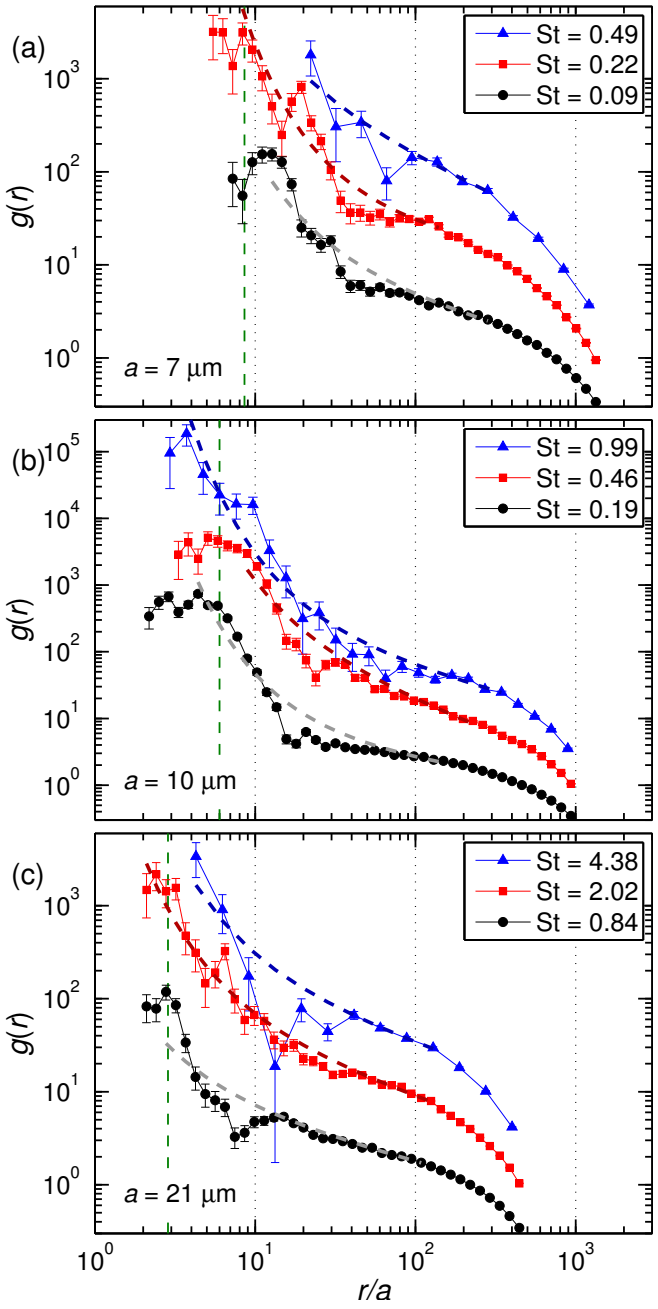

FIG. 2. Measured RDFs $g(r)$ for the three droplet radii: (a) $a = 7$ μm; (b) $a = 10$ μm; (c) $a = 21$ μm. Curves for different Re_λ are shifted vertically for clarity: black circles ($\mathrm{Re}_\lambda = 155$) are at their true height; red squares ($\mathrm{Re}_\lambda = 229$) shifted up by half a decade; blue triangles ($\mathrm{Re}_\lambda = 314$) by a full decade. The dashed lines are fits of Eq. (2) to the curves (with $c_3 = 0$ as explained in the text). Error bars denote intervals of one standard deviation; the green vertical dashed line indicates $r_c \approx 60$ μm below which cross-talk in bin counting due to positioning uncertainty may affect individual bin statistics (more details on these issues are given in the Supplemental Material [34]).

sumed small compared to the smallest turbulence time scale τ_η, i.e. $\mathrm{St} \ll 1$. The flow can then be described by a velocity gradient $\Gamma_{ij} = \partial U_i/\partial x_j$ constant in space and time, with U_i the flow velocity in the x_i direction in the undisturbed situation without the spheres. Since the velocities v of the spheres will remain modest, their Reynolds numbers $\mathrm{Re}_p = 2av/\nu \ll 1$ (ν is the kinematic viscosity of air) and a Stokes flow description is warranted. The motion of two spheres in Stokes flow with constant Γ_{ij} is a classical problem [38–42]. We add inertia as a per-particle force $F_i^{(\#)} = \frac{4}{3}\pi a^3 \rho_p \, \mathrm{d}v_i^{(\#)}/\mathrm{d}t$ and torque $T_i^{(\#)} = \frac{8}{15}\pi a^5 \rho_p \, \mathrm{d}\omega_i^{(\#)}/\mathrm{d}t$, with time t, angular velocity ω, and $\# = 1, 2$ a particle index for the interacting pair. The relative position $\mathbf{r} = \mathbf{x}^{(2)} - \mathbf{x}^{(1)}$, relative velocity $\mathbf{v} = \mathbf{v}^{(2)} - \mathbf{v}^{(1)}$ and total angular velocity $\boldsymbol{\omega} = \boldsymbol{\omega}^{(1)} + \boldsymbol{\omega}^{(2)}$ are expanded in the small parameter St [5]: $\mathbf{r} = \mathbf{r}^{\{0\}} + \mathrm{St}\,\mathbf{r}^{\{1\}} + \mathrm{St}^2\,\mathbf{r}^{\{2\}} + \ldots$ and similar for $\mathbf{v}$ and $\boldsymbol{\omega}$. The viscous interaction terms have near-field ($r = |\mathbf{r}| \lesssim 3a$) and far-field ($r \gtrsim 3a$) series expansions [13], the latter of which we shall use given that the measurements are for this range only. The far-field expansion is a power series in r/a with negative exponents, where only the dominant terms of order $(r/a)^{-\beta}$ with $\beta \in \{0, 1\}$ are retained. A drift–diffusion model [5, 14] to include the effects of turbulence finally leads to the following expression for the RDF:

$$g(r) \propto \underbrace{\exp\left[\frac{c_3}{6}\left(\frac{a}{r}\right)^6\right]}_{①} \cdot \underbrace{\exp\left(c_2 \mathrm{St}^2 \frac{a}{r}\right)}_{②} \cdot \underbrace{\left(\frac{a}{r}\right)^{c_1 \mathrm{St}^2}}_{③}, \quad (2)$$

where $c_{1,2,3}$ are constants which are dependent on the turbulence properties and on St. Term ① of Eq. (2) represents the dominant far-field term for HI of finite-size non-inertial particles leading to clustering, a result fully in line with Ref. [14]. Term ② is a new result obtained here; it represents the extra clustering due to HI of inertial particles at small r. Note that both ① and ② reduce rapidly to 1 at large r; the HI terms are only active on relatively short distances r. Finally, term ③ represents the original power-law behaviour derived for non-HI inertial particles [5]. The limit of non-HI inertial particles is correctly recovered by setting $c_2 = c_3 = 0$ (no HI terms).

To further substantiate and interpret these experimental and analytical results we determine values of the coefficients $c_{1,2}$ as follows: we first fit the power-law term involving c_1 to the appropriate range in r, then fit to determine c_2 at that particular c_1. The term involving c_3 only contributes close to contact [14] (not accessible with our measurements) where our far-field approach breaks down. Furthermore, the experiment has lower statistical accuracy at the smallest r values as evidenced by the larger error bars. These fits are included in Fig. 2 with dashed lines. A direct fit of Eq. (2) is complicated here given noticeable flattening compared to the predicted power-law scaling at lower r in several of the curves. This effect could be due to polydispersity: Refs. [5, 43] have demonstrated that for a bidisperse collection the power-

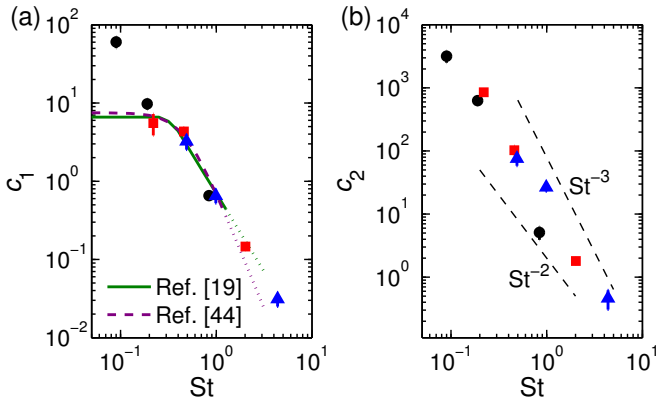

FIG. 3. Coefficients (a) c_1 and (b) c_2 as a function of St, obtained from the experiments. As in Fig. 2, black circles are at $Re_\lambda = 155$; red squares at $Re_\lambda = 229$ and blue triangles at $Re_\lambda = 314$. In (a) two reference DNS results are included [19, 44]; the dotted lines are straightforward extensions of the reported trends to higher St.

law scaling levels off below some separation distance; the effect was found to be prominent even for small differences in diameter and is thus expected to be present even for the current narrow droplet size spectra. The model incorporating differential acceleration of bidisperse droplets [5] predicts a cutoff length which is estimated to be typically a factor two smaller than where we observe the flattening. The extension due to differential gravitational settling of unequal-sized droplets [28] is negligibly small compared to the differential acceleration effect. Additionally, particularly in the black curves the slope change is at smaller r, where we presume that higher-order terms, excluded in the derivation of Eq. (2), are more prominent compared to the other cases.

The values of c_1 and c_2 are plotted in Fig. 3. Beginning with c_1 (Fig. 3a), we compare the experimental results to DNS (without HI) [19, 44]. As predicted by theory (without HI) [5], the DNS [19, 44] show that c_1 (as defined here) is independent of St for small St values. Ref. [19] reports $c_1 = 6.6$ for $\mathrm{St} \lesssim 0.3$ and $c_1 = 0.7St^{-2}$ for $\mathrm{St} \gtrsim 0.3$. The results of Ref. [44] can be parametrized as $c_1 = 0.75/(0.1 + St^3)$ (see also [19]). The current experiments match these results, apart from the data point at $\mathrm{St} = 0.09$. Curiously, this point displays more clustering than expected based on DNS and theory. It may well be that HI (excluded from the DNS and earlier theory) steepens the power-law scaling too. We do want to note that the low-St prediction for the original inertial clustering problem (without HI, which implies $c_1 \sim \mathrm{St}^0$) to this date only has numerical validations, e.g. [19, 44], but no direct experimental confirmation. Unfortunately, the range $\mathrm{St} \ll 1$ is the hardest to access with experiments given the complications of illuminating and detecting such small droplets. Furthermore, this droplet population displays the largest relative spread in terms of St; smearing-out of effects sensitive to St is unavoidable. For the highest St the trend derived from the current experimental results is closer to $c_1 \propto \mathrm{St}^{-2}$ than to $c_1 \propto \mathrm{St}^{-3}$, thus favoring the high-St trend observed in Ref. [19] over that of [44]. There are no signs of dependence on Re_λ.

The measured c_2 (Fig. 3b) display a similar trend to c_1: approximate power-law scalings with exponents between -2 and -3. Thus for increasing St a gradual reduction of the importance of the clustering term $\exp(c_2 \mathrm{St}^2 a/r)$ is expected. We cannot draw conclusions about the lowest $\mathrm{St} = 0.09$, which is inconvenient given that the current theory is formally derived in the limit $\mathrm{St} \ll 1$. However, given that the result of a power-law scaling for the RDF of non-interacting particles has been found to be appropriate at higher St too, we expect that the current theory remains valid also at larger St as it is based on the same propositions. So we speculate that we predominantly measure the large-St branch of $c_2(\mathrm{St})$ here, where $c_2 \sim \mathrm{St}^\alpha$ should scale with an exponent $\alpha < -2$ for the HI clustering to eventually vanish for large enough St. This is a plausible result considering that the weak hydrodynamic interaction velocity should be inconsequential for large and/or heavy enough particles (i.e. with large enough St). The dependence of c_2 on St in the small-St limit is definitely an important question, yet one that is hard to answer given the experimental challenges mentioned before. We finally remark that there are no signs of a significant dependence of c_2 on Re_λ.

We have described a small-scale clustering mechanism for inertial particles in turbulence driven by HI. High-resolution position measurements of droplets in turbulence support this effect. The subsequent enhancement of droplet collision probabilities is of paramount importance for precipitation formation modelling. HI is typically treated exclusively as a repulsive term in models [15–17, 45, 46] and in DNS studies of turbulent flows with point particles [47–51]. The current study reveals that a more extensive description of HI is required to correctly incorporate the attractive effects into DNS and theoretical models to achieve a correct evaluation of droplet collision probabilities.

This work is supported by the Dutch Foundation for Fundamental Research on Matter (FOM) (Program 112 “Droplets in Turbulent Flow”).

* r.p.j.kunnen@tue.nl

[1] M. R. Maxey, J. Fluid Mech. **174**, 441 (1987).
[2] J. K. Eaton and J. R. Fessler, Int. J. Multiphase Flow **20**, 169 (1994).
[3] T. Elperin, N. Kleeorin, and I. Rogachevskii, Phys. Rev. Lett. **77**, 5373 (1996).
[4] E. Balkovsky, G. Falkovich, and A. Fouxon, Phys. Rev. Lett. **86**, 2790 (2001).

[5] J. Chun, D. L. Koch, S. L. Rani, A. Ahluwalia, and L. R. Collins, J. Fluid Mech. **536**, 219 (2005).

[6] J. P. L. C. Salazar, J. de Jong, L. Cao, S. H. Woodward, H. Meng, and L. R. Collins, J. Fluid Mech. **600**, 245 (2008).

[7] F. Toschi and E. Bodenschatz, Annu. Rev. Fluid Mech. **41**, 375 (2009).

[8] E.-W. Saw, R. A. Shaw, J. P. L. C. Salazar, and L. R. Collins, New J. Phys. **14**, 105031 (2012).

[9] S. Sumbekova, A. Cartellier, A. Aliseda, and M. Bourgoin, Phys. Rev. Fluids **2**, 024302 (2017).

[10] R. A. Shaw, Annu. Rev. Fluid Mech. **35**, 183 (2003).

[11] B. J. Devenish, P. Bartello, J.-L. Brenguier, L. R. Collins, W. W. Grabowski, R. H. A. IJzermans, S. P. Malinowski, M. W. Reeks, J. C. Vassilicos, L.-P. Wang, and Z. Warhaft, Q. J. R. Meteorol. Soc. **138**, 1401 (2012).

[12] W. W. Grabowski and L.-P. Wang, Annu. Rev. Fluid Mech. **45**, 293 (2013).

[13] S. Kim and S. J. Karrila, *Microhydrodynamics* (Butterworth–Heinemann, Boston, MA, 1991).

[14] B. K. Brunk, D. L. Koch, and L. W. Lion, Phys. Fluids **9**, 2670 (1997).

[15] I. Langmuir, J. Meteor. **5**, 175 (1948).

[16] H. Pruppacher and J. Klett, *Microphysics of Clouds and Precipitation* (Kluwer Academic Publishers, 1997).

[17] M. B. Pinsky, A. P. Khain, and M. Shapiro, J. Atmos. Sci. **64**, 2462 (2007).

[18] D. A. McQuarrie, *Statistical Mechanics* (Harper & Row, London, 1976).

[19] E.-W. Saw, J. P. L. C. Salazar, L. R. Collins, and R. A. Shaw, New J. Phys. **14**, 105030 (2012).

[20] W. Hwang and J. K. Eaton, Exp. Fluids **36**, 444 (2004).

[21] K. Chang, G. P. Bewley, and E. Bodenschatz, J. Fluid Mech. **692**, 464 (2012).

[22] G. P. Bewley, E.-W. Saw, and E. Bodenschatz, New J. Phys. **15**, 083051 (2013).

[23] G. Bertens, D. van der Voort, H. Bocanegra Evans, and W. van de Water, Exp. Fluids **56**, 89 (2015).

[24] C. N. Davies and P. K. P. Cheah, J. Aerosol Sci. **15**, 719 (1984).

[25] H. Bocanegra Evans, N. Dam, G. Bertens, D. van der Voort, and W. van de Water, Phys. Rev. Lett. **117**, 164501 (2016).

[26] H. Bocanegra Evans, N. Dam, D. van der Voort, G. Bertens, and W. van de Water, Rev. Sci. Instrum. **86**, 023709 (2015).

[27] O. Ayala, B. Rosa, L.-P. Wang, and W. W. Grabowski, New J. Phys. **10**, 075015 (2008).

[28] J. Lu, H. Nordsiek, and R. A. Shaw, New J. Phys. **12**, 123030 (2010).

[29] E. J. P. Woittiez, H. J. J. Jonker, and L. M. Portela, J. Atmos. Sci. **66**, 1926 (2009).

[30] C. T. Crowe, M. Sommerfeld, and Y. Tsuji, *Multiphase Flows with Droplets and Particles* (CRC Press, Boca Raton, 1998).

[31] H. G. Maas, A. Gruen, and D. Papantoniou, Exp. Fluids **15**, 133 (1993).

[32] N. A. Malik, T. Dracos, and D. A. Papantoniou, Exp. Fluids **15**, 279 (1993).

[33] B. Lüthi, A. Tsinober, and W. Kinzelbach, J. Fluid Mech. **528**, 87 (2005).

[34] See Supplemental Material [url], which includes Refs. [52–55].

[35] J. Lu, H. Nordsiek, E. W. Saw, and R. A. Shaw, Phys. Rev. Lett. **104**, 184505 (2010).

[36] J. Lu and R. A. Shaw, Phys. Fluids **27**, 065111 (2015).

[37] The model derived in [35] results in an RDF with a charge-induced multiplicative factor $\exp[-(2\tau_\eta\tau_p kq^2)/(3B_{nl}mr^3)]$ with m the droplet mass, q its charge, $k = 9.0\times10^9$ N m^2/C^2 Coulomb's constant and B_{nl} a nonlocal diffusion coefficient treated in more detail in the Supplemental Material [34]. We can rewrite this factor as $\exp[-(2/3B_{nl})(r_c^*/r)^3]$ with r_c^* a measure for the transition lengthscale between turbulence-dominated ($r > r_c^*$) and charge-dominated droplet interaction ($r < r_c^*$), which in terms of the principal experiment paramaters scales as $r_c^* = [kq^2/(a\rho_f\sqrt{\nu\epsilon})]^{1/3}$. The model of [36] provides a transition scale with an identical dependence on these parameters. Note that in this model r_c^* should go down as ϵ is increased; in the current experimental results we instead observe an increased range of clustering as ϵ is increased. Thus electrical charging of droplets cannot explain the trends in clustering observed here.

[38] C. J. Lin, K. J. Lee, and N. F. Sather, J. Fluid Mech. **43**, 35 (1970).

[39] G. K. Batchelor and J. T. Green, J. Fluid Mech. **56**, 375 (1972).

[40] G. K. Batchelor and J. T. Green, J. Fluid Mech. **56**, 401 (1972).

[41] H. Brenner and M. E. O'Neill, Chem. Engng Sci. **27**, 1421 (1972).

[42] P. A. Arp and S. G. Mason, J. Colloid Interface Sci. **61**, 21 (1977).

[43] J. Bec, A. Celani, M. Cencini, and S. Musacchio, Phys. Fluids **17**, 073301 (2005).

[44] G. Falkovich and A. Pumir, J. Atmos. Sci. **64**, 4497 (2007).

[45] A. P. Khain, M. B. Pinsky, M. Shapiro, and A. Pokrovsky, J. Atmos. Sci. **58**, 2571 (2001).

[46] L.-P. Wang, O. Ayala, and W. W. Grabowski, J. Atmos. Sci. **62**, 1255 (2005).

[47] L.-P. Wang, O. Ayala, S. E. Kasprzak, and W. W. Grabowski, J. Atmos. Sci. **62**, 2433 (2005).

[48] L.-P. Wang, O. Ayala, B. Rosa, and W. W. Grabowski, New J. Phys. **10**, 075013 (2008).

[49] B. Rosa, L.-P. Wang, M. R. Maxey, and W. W. Grabowski, J. Comput. Phys. **230**, 8109 (2011).

[50] R. Onishi, K. Takahashi, and J. C. Vassilicos, J. Comput. Phys. **242**, 809 (2013).

[51] R. Onishi, K. Matsuda, and K. Takahashi, J. Atmos. Sci. **72**, 2591 (2015).

[52] E. W. Saw, R. A. Shaw, S. Ayyalasomayajula, P. Y. Chuang, and Á. Gylfason, Phys. Rev. Lett. **100**, 214501 (2008).

[53] R. Bordás, Ch. Roloff, D. Thévenin, and R. A. Shaw, New J. Phys. **15**, 045010 (2013).

[54] E. D. Siggia, Phys. Fluids **24**, 1934 (1981).

[55] J. Hierro and C. Dopazo, Phys. Fluids **15**, 3434 (2003).

Supplemental Material to "Extreme Small-Scale Clustering of Droplets in Turbulence Driven by Hydrodynamic Interactions"

M. A. Yavuz, R. P. J. Kunnen,* G. J. F. van Heijst, and H. J. H. Clercx
Fluid Dynamics Laboratory, Department of Applied Physics and J. M. Burgers Center for Fluid Dynamics, Eindhoven University of Technology, P.O. Box 513, 5600 MB Eindhoven, The Netherlands
(Dated: June 11, 2018)

STATISTICAL UNCERTAINTY AND CONVERGENCE OF THE RDF MEASUREMENTS

The total measurement duration per experiment is detailed in Table I. Image acquisition in the experiment is done at 1 kHz in several batches of 9600 images each; batch size is limited by the camera memory. We express the total measurement duration also in terms of the turbulence integral timescale $T = \frac{3}{2}(u')^2/\epsilon$. It is clear that many uncorrelated independent samples of the total droplet field are recorded. In fact, even at such high recording frequency droplets are displaced by distances considerably larger than at least the smaller bin widths Δr_i so that correlated double counting in these bins (crucial for the current results) is very rare.

To assess the statistical error in the RDF, we employ the assumption that events of finding two droplets within the measurement volume V_0 separated by a distance r within a certain spherical-shell bin of mean radius r_i can be described with Poisson statistics; a fair assumption here given that correlations between events will be minimal. This approach is the default for treating such data [1–3]. It means that based on Eq. (1) of the main text we may estimate the standard deviation σ_{N_i} of the pairs counted per bin as $\sigma_{N_i} = \sqrt{N_i}$ (similarly $\sigma_N = \sqrt{N}$) and thus find for the standard deviation $\sigma_{g(r_i)}$ of the RDF with standard error propagation:

$$\sigma_{g(r_i)} = \sqrt{\left(\sigma_{N_i}\frac{\partial g}{\partial N_i}\right)^2 + \left(\sigma_N \frac{\partial g}{\partial N}\right)^2} = \frac{\sqrt{N_i}}{N}\frac{V}{\Delta V_i}\sqrt{1+\frac{N_i}{N}}\,. \tag{1}$$

Note that since N is large the final term $\sqrt{1+N_i/N}$ can be safely left out without appreciable changes to the result. We have plotted the RDF results with error bars of $\pm 1\sigma_{g(r_i)}$. Obviously, the leftmost points of each RDF curve (at small r) are typically based on rather small numbers of counts. That is why the corresponding error bars have lengths up to 70% of the RDF values; a fact that is obscured somewhat by the use of a logarithmically scaled ordinate with a rather large numerical range. The statistical convergence has been further validated by also processing partial intervals of the total data range per experiment and comparing the results with satisfactory agreement.

We have evaluated the performance of the 3D positioning *a posteriori*. The realized error in position is 15 to 20 μm (depending on conditions), i.e. about one droplet diameter for the smaller droplets and considerably less than one diameter for the largest droplets. There is some cross-talk experienced between the first few bins for RDF counting given the realized error in 3D positioning (leading to uncertainty in r) of up to 15 to 20 μm. Pairs counted in one bin may belong to another, causing some wiggles in the RDF plots for the smallest r values (the first few bins). However, the bin size rapidly increases to the right (larger r). This cross-talk effect is reduced well within the range of r where

TABLE I. Measurement time t_{meas} per experiment, expressed in dimensional form as well as normalized with the integral timescale T.

Re_λ	T (s)	a (μm)	Batches	t_{meas} (s)	t_{meas}/T
155	0.45	7	7	67.2	149
155	0.45	10	10	96.0	213
155	0.45	21	10	96.0	213
229	0.24	7	14	134.4	560
229	0.24	10	11	105.6	440
229	0.24	21	10	96.0	440
314	0.15	7	10	96.0	640
314	0.15	10	10	96.0	640
314	0.15	21	11	105.6	704

we observe the anomalous increase of the RDF; we find that cross-talk is relevant up to $r_c \approx 60$ μm while the observed anomalous increase is based on hundreds to thousands of droplet pairs at small separations r but larger than r_c.

DETAILED DERIVATION OF EQ. (2) IN THE MAIN TEXT

The motion of two spheres in Stokes flow with constant velocity gradient tensor $\Gamma_{ij} = \partial U_i/\partial x_j$ is a classical problem [4–8]. We start at the equations of motion for a pair of small spherical particles in Stokes flow in the mobility-matrix formulation [9]:

$$\begin{bmatrix} \mathbf{U}(\mathbf{x}^{(1)}) - \mathbf{v}^{(1)} \\ \mathbf{U}(\mathbf{x}^{(2)}) - \mathbf{v}^{(2)} \\ \boldsymbol{\Omega} - \boldsymbol{\omega}^{(1)} \\ \boldsymbol{\Omega} - \boldsymbol{\omega}^{(2)} \end{bmatrix} = \begin{bmatrix} \mathbf{a}^{(11)} & \mathbf{a}^{(12)} & \tilde{\mathbf{b}}^{(11)} & \tilde{\mathbf{b}}^{(12)} & \tilde{\mathbf{g}}^{(1)} \\ \mathbf{a}^{(21)} & \mathbf{a}^{(22)} & \tilde{\mathbf{b}}^{(21)} & \tilde{\mathbf{b}}^{(22)} & \tilde{\mathbf{g}}^{(2)} \\ \mathbf{b}^{(11)} & \mathbf{b}^{(12)} & \mathbf{c}^{(11)} & \mathbf{c}^{(12)} & \tilde{\mathbf{h}}^{(1)} \\ \mathbf{b}^{(21)} & \mathbf{b}^{(22)} & \mathbf{c}^{(21)} & \mathbf{c}^{(22)} & \tilde{\mathbf{h}}^{(2)} \end{bmatrix} \cdot \begin{bmatrix} \mu^{-1}\mathbf{F}^{(1)} \\ \mu^{-1}\mathbf{F}^{(2)} \\ \mu^{-1}\mathbf{T}^{(1)} \\ \mu^{-1}\mathbf{T}^{(2)} \\ \mathbf{S} \end{bmatrix}, \tag{2}$$

with $\mathbf{x}^{(1)}$ the position of particle 1, $\mathbf{v}^{(1)}$ its velocity, $\boldsymbol{\omega}^{(1)}$ its angular velocity, and $\mathbf{F}^{(1)}$ and $\mathbf{T}^{(1)}$ the force and torque exerted on particle 1 by the fluid, respectively, and similar for particle 2. The undisturbed flow $\mathbf{U}$ at position $\mathbf{x}$ is $U_i(\mathbf{x}) = U_{0,i} + \epsilon_{ijk}\Omega_j x_k + S_{ij}x_j = U_{0,i} + \Gamma_{ij}x_j$, with summation over repeated indices. The decomposition of Γ_{ij} into rate-of-strain $S_{ij} = \frac{1}{2}(\Gamma_{ij} + \Gamma_{ji})$ and rotation $R_{ij} = \frac{1}{2}(\Gamma_{ij} - \Gamma_{ji})$ parts is used; furthermore $\Omega_i = -\epsilon_{ijk}R_{jk}$. Rank-2 tensors $\mathbf{a}$, $\mathbf{b}$, $\tilde{\mathbf{b}}$ and $\mathbf{c}$ and rank-3 tensors $\tilde{\mathbf{g}}$ and $\tilde{\mathbf{h}}$ describe the interparticle interactions and are tabulated with accompanying symmetry relations [9]. Finally, μ is the dynamic viscosity of the fluid.

We define relative coordinates $\mathbf{r} = \mathbf{x}^{(2)} - \mathbf{x}^{(1)}$, relative velocity $\mathbf{v} = \mathbf{v}^{(2)} - \mathbf{v}^{(1)}$ and total angular velocity $\boldsymbol{\omega} = \boldsymbol{\omega}^{(1)} + \boldsymbol{\omega}^{(2)}$, for which follows from (2) and the tensor symmetries that

$$\begin{aligned} v_i = {} & \Gamma_{ij}r_j + \mu^{-1}\left(a_{ij}^{(12)} - a_{ij}^{(11)}\right)\left(F_j^{(2)} - F_j^{(1)}\right) \\ & + \mu^{-1}\left(b_{ij}^{(12)} - b_{ij}^{(11)}\right)\left(T_j^{(1)} + T_j^{(2)}\right) + \left(\tilde{g}_{ijk}^{(1)} - \tilde{g}_{ijk}^{(2)}\right)S_{jk}\,, \end{aligned} \tag{3a}$$

$$\begin{aligned} \omega_i = {} & 2\Omega_i + \mu^{-1}\left(b_{ij}^{(11)} - b_{ij}^{(12)}\right)\left(F_j^{(2)} - F_j^{(1)}\right) \\ & - \mu^{-1}\left(c_{ij}^{(11)} + c_{ij}^{(12)}\right)\left(T_j^{(1)} + T_j^{(2)}\right) - \left(\tilde{h}_{ijk}^{(1)} + \tilde{h}_{ijk}^{(2)}\right)S_{jk}\,. \end{aligned} \tag{3b}$$

The interaction tensor terms can be rewritten [9]:

$$\begin{aligned} v_i = {} & \Gamma_{ij}r_j + (6\pi a\mu)^{-1}\left[\mathcal{A}\frac{r_i r_j}{r^2} + \mathcal{B}\left(\delta_{ij} - \frac{r_i r_j}{r^2}\right)\right]\left(F_j^{(2)} - F_j^{(1)}\right) \\ & + (4\pi a^2\mu)^{-1}\mathcal{C}\epsilon_{ijk}\frac{r_k}{r}\left(T_j^{(1)} + T_j^{(2)}\right) - 2a\left[\mathcal{D}\frac{r_i r_j}{r^2} + \mathcal{E}\left(\delta_{ij} - \frac{r_i r_j}{r^2}\right)\right]S_{jk}\frac{r_k}{r}\,, \end{aligned} \tag{4a}$$

$$\begin{aligned} \omega_i = {} & 2\Omega_i - (4\pi a^2\mu)^{-1}\mathcal{C}\epsilon_{ijk}\frac{r_k}{r}\left(F_j^{(2)} - F_j^{(1)}\right) \\ & - (8\pi a^3\mu)^{-1}\left[\mathcal{F}\frac{r_i r_j}{r^2} + \mathcal{G}\left(\delta_{ij} - \frac{r_i r_j}{r^2}\right)\right]\left(T_j^{(1)} + T_j^{(2)}\right) + \mathcal{H}\left(\epsilon_{jil}\frac{r_l r_k}{r^2} + \epsilon_{kil}\frac{r_l r_j}{r^2}\right)S_{jk}\,. \end{aligned} \tag{4b}$$

The (dimensionless) terms $\mathcal{A}, \mathcal{B}, \ldots, \mathcal{H}$ can be derived from the tables in [9].

Inertia is introduced as $F_i^{(1)} = m\,\mathrm{d}v_i^{(1)}/\mathrm{d}t$ with time t and droplet mass $m = \frac{4}{3}\pi\rho_p a^3$ (ρ_p is its density), and $T_i^{(1)} = I\,\mathrm{d}\omega_i^{(1)}/\mathrm{d}t$ with droplet moment of inertia $I = \frac{8}{15}\pi\rho_p a^5$. We introduce the droplet relaxation time $\tau_p = \frac{2}{9}\rho_p a^2/\mu$ and the Stokes number $\mathrm{St} = \tau_p/\tau_\eta$ with Kolmogorov time τ_η. Henceforth we write nondimensionalized variables (scaling length with a and time with τ_η) with a hat, e.g., $\hat{r} = r/a$. Equation (4) can be rewritten as

$$\begin{aligned} \hat{v}_i = {} & \hat{\Gamma}_{ij}\hat{r}_j + \mathrm{St}\left[\mathcal{A}\frac{\hat{r}_i\hat{r}_j}{\hat{r}^2} + \mathcal{B}\left(\delta_{ij} - \frac{\hat{r}_i\hat{r}_j}{\hat{r}^2}\right)\right]\frac{\mathrm{d}\hat{v}_j}{\mathrm{d}\hat{t}} + \tfrac{3}{5}\mathrm{St}\,\mathcal{C}\,\epsilon_{ijk}\frac{\hat{r}_k}{\hat{r}}\frac{\mathrm{d}\hat{\omega}_j}{\mathrm{d}\hat{t}} \\ & - 2\left[\mathcal{D}\frac{\hat{r}_i\hat{r}_j}{\hat{r}^2} + \mathcal{E}\left(\delta_{ij} - \frac{\hat{r}_i\hat{r}_j}{\hat{r}^2}\right)\right]\hat{S}_{jk}\frac{\hat{r}_k}{\hat{r}}\,, \end{aligned} \tag{5a}$$

$$\hat{\omega}_i = 2\hat{\Omega}_i - \tfrac{3}{2}\mathrm{St}\,\mathcal{C}\,\epsilon_{ijk}\frac{\hat{r}_k}{\hat{r}}\frac{\mathrm{d}\hat{v}_j}{\mathrm{d}\hat{t}} - \tfrac{3}{10}\mathrm{St}\left[\mathcal{F}\frac{\hat{r}_i\hat{r}_j}{\hat{r}^2} + \mathcal{G}\left(\delta_{ij} - \frac{\hat{r}_i\hat{r}_j}{\hat{r}^2}\right)\right]\frac{\mathrm{d}\hat{\omega}_j}{\mathrm{d}\hat{t}} - 2\mathcal{H}\epsilon_{jil}\frac{\hat{r}_l\hat{r}_k}{\hat{r}^2}\hat{S}_{jk}\,, \tag{5b}$$

where we have evaluated the sum in the final bracketed term of Eq. 4b by exploiting the symmetry of $\hat{S}_{jk}$.

As in Ref. [10], we expand $\hat{\mathbf{r}}$, $\hat{\mathbf{v}}$ and $\hat{\boldsymbol{\omega}}$ in the small parameter St: $\hat{r}_i = \hat{r}_i^{\{0\}} + \mathrm{St}\,\hat{r}^{\{1\}} + \mathrm{St}^2\hat{r}^{\{2\}} + \cdots$ and similar for $\hat{v}_i$ and $\hat{\omega}_i$. We retain terms up to $O(\mathrm{St})$ and set afterward $\hat{r}^{\{0\}} \to \hat{r}$, $\hat{r}^{\{1\}} \to 0$. Herewith we obtain $\hat{v}_i^{\{1\}}$, the $O(\mathrm{St})$ correction to the relative velocity. The series $\mathcal{A}$, $\mathcal{B}$, …, $\mathcal{H}$ can be expanded in St too, but their $O(\mathrm{St})$ parts only contribute in the equations at $O(\mathrm{St}^2)$ and higher.

Gathering terms of the same order in St, we find to $O(\mathrm{St}^0)$:

$$\hat{v}_i^{\{0\}} = \hat{\Gamma}_{ij}\hat{r}_j - 2\left[\mathcal{D}\frac{\hat{r}_i\hat{r}_j}{\hat{r}^2} + \mathcal{E}\left(\delta_{ij} - \frac{\hat{r}_i\hat{r}_j}{\hat{r}^2}\right)\right]\hat{S}_{jk}\frac{\hat{r}_k}{\hat{r}}\,, \tag{6a}$$

$$\hat{\omega}_i^{\{0\}} = 2\hat{\Omega}_i - 2\mathcal{H}\epsilon_{jil}\frac{\hat{r}_l\hat{r}_k}{\hat{r}^2}\hat{S}_{jk}\,. \tag{6b}$$

For $\hat{v}_i^{\{1\}}$ we gather to $O(\mathrm{St})$:

$$\hat{v}_i^{\{1\}} = \left[\mathcal{A}\frac{\hat{r}_i\hat{r}_j}{\hat{r}^2} + \mathcal{B}\left(\delta_{ij} - \frac{\hat{r}_i\hat{r}_j}{\hat{r}^2}\right)\right]\frac{\mathrm{d}\hat{v}_j^{\{0\}}}{\mathrm{d}\hat{t}} + \tfrac{3}{5}\,\mathcal{C}\,\epsilon_{ijk}\frac{\hat{r}_k}{\hat{r}}\frac{\mathrm{d}\hat{\omega}_j^{\{0\}}}{\mathrm{d}\hat{t}}\,. \tag{7}$$

We thus do not need $\hat{\omega}_i^{\{1\}}$ to get the desired expression for $\hat{v}_i^{\{1\}}$.

Ref. 11 derive a drift–diffusion model to statistically include the effects of turbulence. They introduce the following equation for the mean particle drift velocity $\hat{v}_i^f$:

$$\hat{v}_i^f = -\int_{-\infty}^{0}\left\langle \hat{v}_i(\hat{t}')\frac{\partial\hat{v}_j}{\partial\hat{r}_j}(0)\right\rangle \mathrm{d}\hat{t}'\,, \tag{8}$$

where angular brackets denote ensemble averaging. The insertion of (6) into (8) and the description of correlations $\left\langle \hat{S}_{ij}(\hat{t}')\hat{S}_{kl}(0)\right\rangle$ and $\left\langle \hat{R}_{ij}(\hat{t}')\hat{R}_{kl}(0)\right\rangle$ in terms of strain and vorticity magnitudes $\hat{S}^2 = \hat{R}^2 = \frac{1}{2}$ with corresponding correlation times $\hat{\tau}_S$ and $\hat{\tau}_R$ has been detailed in [11]. We recover the same $O(\mathrm{St}^0)$ term:

$$\hat{v}_i^{f\{0\}} = \tfrac{4}{15}\hat{S}^2\hat{\tau}_S\left[\hat{r}\frac{\mathrm{d}\mathcal{D}}{\mathrm{d}\hat{r}} + 2\mathcal{D} - 3\mathcal{E}\right]\left(1 - 2\frac{\mathcal{D}}{\hat{r}}\right)\frac{\hat{r}_i}{\hat{r}}\,, \tag{9}$$

(The corresponding notation in Ref. [11] is $A(r) = 2\mathcal{D}/\hat{r}$ and $B(r) = 2\mathcal{E}/\hat{r}$; after this substitution the formulations are identical). The mean drift velocity is negative (particles converge) and is $O(\hat{r}^{-6}\hat{r}_i)$ in the far field [11].

To obtain the $O(\mathrm{St})$ contribution to arbitrary precision in $\hat{r}$, the time derivatives in (7) can be obtained by differentiating (6), leading to a multitude of contributions. Here we restrict ourselves to the dominant far-field contributions, dropping contributions $O(\hat{r}^{-\beta})$ for $\beta \geq 2$. The series $\mathcal{A}, \mathcal{B}, \ldots, \mathcal{H}$ reduce to [9]

$$\mathcal{A} = -1 + \tfrac{3}{2}\hat{r}^{-1} + O(\hat{r}^{-3})\,;\ \mathcal{B} = -1 + \tfrac{3}{4}\hat{r}^{-1} + O(\hat{r}^{-3})\,;\ \mathcal{C} = O(\hat{r}^{-2})\,;\ \mathcal{D} = O(\hat{r}^{-2})\,, \tag{10a}$$

$$\mathcal{E} = O(\hat{r}^{-4})\,;\ \mathcal{F} = 1 + O(\hat{r}^{-3})\,;\ \mathcal{G} = 1 + O(\hat{r}^{-3})\,;\ \mathcal{H} = O(\hat{r}^{-3})\,. \tag{10b}$$

We thus obtain the following reduced forms and time derivatives of Eq. (6):

$$\hat{v}^{\{0\}} = \hat{\Gamma}_{ij}\hat{r}_j\,;\quad \frac{\mathrm{d}\hat{v}_i^{\{0\}}}{\mathrm{d}\hat{t}} = \hat{\Gamma}_{ij}\frac{\mathrm{d}\hat{r}}{\mathrm{d}\hat{t}} = \hat{\Gamma}_{ij}\hat{v}_j^{\{0\}} = \hat{\Gamma}_{ij}\hat{\Gamma}_{jk}\hat{r}_k\,, \tag{11a}$$

$$\hat{\omega}_i^{\{0\}} = 2\hat{\Omega}_i\,;\quad \frac{\mathrm{d}\hat{\omega}_i^{\{0\}}}{\mathrm{d}\hat{t}} = 0\,. \tag{11b}$$

We thus find for the relative velocity to $O(\mathrm{St})$:

$$\hat{v}_i^{\{1\}} = (\mathcal{A}-\mathcal{B})\frac{\hat{r}_i\hat{r}_j}{\hat{r}^2}\frac{\mathrm{d}\hat{v}_j^{\{0\}}}{\mathrm{d}\hat{t}} + \mathcal{B}\frac{\mathrm{d}\hat{v}_i^{\{0\}}}{\mathrm{d}\hat{t}} = \tfrac{3}{4}\hat{r}^{-1}\frac{\hat{r}_j\hat{r}_l}{\hat{r}^2}\hat{\Gamma}_{jk}\hat{\Gamma}_{kl}\hat{r}_i + (\tfrac{3}{4}\hat{r}^{-1}-1)\hat{\Gamma}_{ij}\hat{\Gamma}_{jk}\hat{r}_k\,. \tag{12}$$

Formally, to obtain the $O(\mathrm{St})$ contribution to the drift velocity we should consider cross terms of $\hat{v}_i^{\{0\}}$ and $\hat{v}_i^{\{1\}}$ in (8), giving correlations of the form $\left\langle \hat{\Gamma}_{ij}(\hat{t}')\hat{\Gamma}_{kl}(0)\hat{\Gamma}_{lm}(0)\right\rangle$ which are zero by isotropy [10]. Therefore, the $O(\mathrm{St}^2)$ terms are the first nonzero corrections, as in [10]. We insert

$$\frac{\partial\hat{v}_i^{\{1\}}}{\partial\hat{r}_i} = \tfrac{3}{4}\hat{r}^{-1}\frac{\hat{r}_j\hat{r}_l}{\hat{r}^2}\hat{\Gamma}_{jk}\hat{\Gamma}_{kl} + (\tfrac{3}{4}\hat{r}^{-1}-1)\hat{\Gamma}_{jk}\hat{\Gamma}_{kj}\,, \tag{13}$$

and (12) into (8) and find several contractions of second-order two-time velocity gradient correlations. Analogous to [11] for second-order correlations, we describe these as fourth-order correlations with finite correlation times in turbulence. All fourth-order correlations can be expressed in terms of four independent correlations $\hat{F}_1 = \left\langle \left(\frac{\partial\hat{U}_1}{\partial\hat{x}_1}\right)^4\right\rangle$, $\hat{F}_2 = \left\langle \left(\frac{\partial\hat{U}_1}{\partial\hat{x}_1}\right)^2\left(\frac{\partial\hat{U}_2}{\partial\hat{x}_1}\right)^2\right\rangle$, $\hat{F}_3 = \left\langle \left(\frac{\partial\hat{U}_2}{\partial\hat{x}_1}\right)^4\right\rangle$, and $\hat{F}_4 = \left\langle \left(\frac{\partial\hat{U}_1}{\partial\hat{x}_1}\right)^2\left(\frac{\partial\hat{U}_3}{\partial\hat{x}_2}\right)^2\right\rangle$ [12, 13], to which we assign correlation times $\hat{\tau}_{F_1}$ through $\hat{\tau}_{F_4}$. The following correlations are encountered:

$$\hat{r}_k\frac{\hat{r}_l\hat{r}_n}{\hat{r}^2}\left\langle \hat{\Gamma}_{ij}\hat{\Gamma}_{jk}\hat{\Gamma}_{lm}\hat{\Gamma}_{mn}\right\rangle = (\tfrac{15}{2}\hat{F}_1 - 25\hat{F}_2 + \tfrac{8}{3}\hat{F}_3 + 3\hat{F}_4)\delta_{ik}\hat{r}_k\,,$$

$$\hat{r}_k\left\langle \hat{\Gamma}_{ij}\hat{\Gamma}_{jk}\hat{\Gamma}_{pq}\hat{\Gamma}_{qp}\right\rangle = (20\hat{F}_1 - 60\hat{F}_2 + \tfrac{20}{3}\hat{F}_3)\delta_{ik}\hat{r}_k\,,$$

leading to an expression for $\hat{v}_i^{f\{2\}}$ where we again only retain the principal two orders in $\hat{r}$, i.e., $O(\hat{r}^0)$ and $O(\hat{r}^{-1})$:

$$\begin{aligned}\hat{v}_i^{f\{2\}} = {}& \tfrac{3}{4}\hat{r}^{-1}\hat{r}_i\left[\tfrac{15}{2}\hat{F}_1\hat{\tau}_{F_1} - 25\hat{F}_2\hat{\tau}_{F_2} + \tfrac{8}{3}\hat{F}_3\hat{\tau}_{F_3} + 3\hat{F}_4\hat{\tau}_{F_4}\right]\\ & - \left(1-\tfrac{9}{4}\hat{r}^{-1}\right)\hat{r}_i\left[20\hat{F}_1\hat{\tau}_{F_1} - 60\hat{F}_2\hat{\tau}_{F_2} + \tfrac{20}{3}\hat{F}_3\hat{\tau}_{F_3}\right]\,.\end{aligned} \tag{14}$$

The correlation times cannot be directly measured in the current experiment; here we use that the square-bracketed terms are finite values, to be used as coefficients to link the model to the experimental data. Gathering terms up to $O(\mathrm{St}^2)$ with their principal dependence on $\hat{r}$, we find

$$\hat{v}_i^f = -\left[c_3'\hat{r}^{-6} + \mathrm{St}^2\left(c_1' + c_2'\hat{r}^{-1}\right)\right]\hat{r}_i\,, \tag{15}$$

with constants $c_{1,2,3}'$. The next nonzero contribution in $O(\mathrm{St}^0)$ scales as $\hat{r}^{-9}\hat{r}_i$ and is disregarded. To $O(\mathrm{St}^2)$ higher-order terms with $\hat{r}^{-2}\hat{r}_i$ and so on exist, which could in principle be included, but these are correction terms for small $\hat{r}$ to the dominant terms retained here.

The diffusion term is required to close the drift–diffusion description. Ref. [11] also treat the diffusion term, though their description is found to be unrealistic [10]. Therefore, we adopt the diffusion description of [10], which has also been successfully used to describe clustering of charged particles [14–16]. Their (radial) diffusivity $\hat{d}_{||}^f = B_{nl}\hat{r}^2$ includes a nonlocal diffusion coefficient B_{nl} which is expected to be a function of the flow Reynolds number.

The evaluation of these terms in the radial direction leads to a differential equation for the RDF [10, 11, 14]:

$$\hat{v}^f g - \hat{d}_{||}^f\frac{\mathrm{d}g}{\mathrm{d}\hat{r}} = 0\,. \tag{16}$$

The solution is

$$g(\hat{r}) \propto \exp\left(\frac{c_3}{6\hat{r}^6}\right)\exp\left(\mathrm{St}^2\frac{c_2}{\hat{r}}\right)\hat{r}^{-c_1\mathrm{St}^2}\,, \tag{17}$$

with $c_i = c_i'/B_{nl}$, which is equal to Eq. (2) in the main text. It contains the St^2-dependent power-law result of Ref. [10] with exponential terms for the mutual interations at small $\hat{r}$. Note that this is only valid in the far field. As $\hat{r}$ is reduced, more and more terms of $\hat{v}^f$ should be included; for the smallest $\hat{r} \lesssim 3$ (lubrication regime) a repulsive

interaction dominates and $\hat{v}^f$ rapidly reduces to zero, leading to a finite $g(\hat{r}=2)$ at contact [11]. However, such small separations are out of scope here; they are beyond our experimental capability.

* r.p.j.kunnen@tue.nl

[1] E. W. Saw, R. A. Shaw, S. Ayyalasomayajula, P. Y. Chuang, and Á. Gylfason, Phys. Rev. Lett. **100**, 214501 (2008).
[2] E.-W. Saw, R. A. Shaw, J. P. L. C. Salazar, and L. R. Collins, New J. Phys. **14**, 105031 (2012).
[3] R. Bordás, Ch. Roloff, D. Thévenin, and R. A. Shaw, New J. Phys. **15**, 045010 (2013).
[4] C. J. Lin, K. J. Lee, and N. F. Sather, J. Fluid Mech. **43**, 35 (1970).
[5] G. K. Batchelor and J. T. Green, J. Fluid Mech. **56**, 375 (1972).
[6] G. K. Batchelor and J. T. Green, J. Fluid Mech. **56**, 401 (1972).
[7] H. Brenner and M. E. O'Neill, Chem. Engng Sci. **27**, 1421 (1972).
[8] P. A. Arp and S. G. Mason, J. Colloid Interface Sci. **61**, 21 (1977).
[9] S. Kim and S. J. Karrila, *Microhydrodynamics* (Butterworth–Heinemann, Boston, MA, 1991).
[10] J. Chun, D. L. Koch, S. L. Rani, A. Ahluwalia, and L. R. Collins, J. Fluid Mech. **536**, 219 (2005).
[11] B. K. Brunk, D. L. Koch, and L. W. Lion, Phys. Fluids **9**, 2670 (1997).
[12] E. D. Siggia, Phys. Fluids **24**, 1934 (1981).
[13] J. Hierro and C. Dopazo, Phys. Fluids **15**, 3434 (2003).
[14] J. Lu, H. Nordsiek, E. W. Saw, and R. A. Shaw, Phys. Rev. Lett. **104**, 184505 (2010).
[15] J. Lu, H. Nordsiek, and R. A. Shaw, New J. Phys. **12**, 123030 (2010).
[16] J. Lu and R. A. Shaw, Phys. Fluids **27**, 065111 (2015).